Journal of Power Sources 246 (2014) 548–555

Contents lists available at ScienceDirect

Journal of Power Sources

journal homepage: www.elsevier.com/locate/jpowsour

Molybdenum carbide catalysed hydrogen production from formic acid – A density functional theory study

Qiquan Luo, Tao Wang, Guido Walther, Matthias Beller, Haijun Jiao*

Leibniz-Institut für Katalyse e.V. an der Universität Rostock, Albert-Einstein-Straße 29a, 18059 Rostock, Germany

HIGHLIGHTS

- HCOOH decomposition on β-Mo_2C (101) was investigated using First-principles calculations.
- The decomposition mechanisms were compared with those on Pt group metals.
- CO-free hydrogen formation was found via the formate route dissociation.

GRAPHICAL ABSTRACT

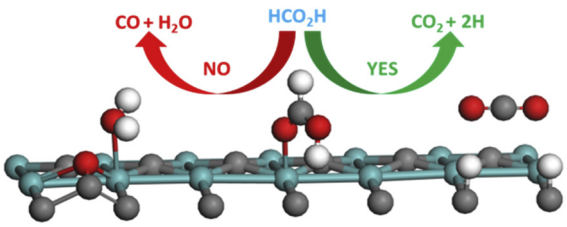

ARTICLE INFO

Article history:
Received 1 April 2013
Received in revised form
25 July 2013
Accepted 28 July 2013
Available online 3 August 2013

Keywords:
DFT
Formic acid
Molybdenum carbide
Hydrogen
CO_2
Catalysis

ABSTRACT

Density functional theory computations have been employed to investigate the decomposition of formic acid (HCO_2H) into CO_2 and hydrogen on the β-Mo_2C(101) surface. The adsorption configurations and energies of the surface intermediates (HCO_2H, CO_2, CO, H_2O, HCO_2, CO_2H, CHO, OH, O and H) have been systematically characterized. Among the different dissociation steps considered, our results showed the formate route ($HCO_2H \rightarrow H + HCO_2$; $HCO_2 \rightarrow H + CO_2$) is the minimum energy path for hydrogen formation and CO_2 has very strong chemisorption. The adsorption and dissociation of formic acid on the Mo_2C(101) surface have been compared with those of Pt group metals.

1. Introduction

Selective and catalytic decomposition of formic acid (FA, HCO_2H) into H_2 and CO_2 is considered as one of the potential chemical processes to satisfy the increasing energy demand, especially in fuel cell, green and clean technologies [1–3]. For FA selective decomposition both heterogeneous [4–7] and homogeneous [8–12] catalysts have been used. Recently, Flaherty et al. studied FA decomposition on molybdenum carbide and found that C-modified Mo(110) and C–Mo(110) are up to 15 times more selective than pure Mo(110) for H_2 formation [13]. Koós and Solymosi reported that the highly stable molybdenum carbide (Mo_2C) catalyst prepared from the reaction of MoO_3 with a multiwall carbon nanotube and carbon Norit can selectively decompose FA into CO-free H_2 at 373–473 K [14]. Cui et al. reported that Pd catalysts supported on Mo_2C which is supported on multiwall carbon nanotube has much higher electrocatalytic activity and stability for FA electroxidation than only Mo_2C catalyst supported on multiwall carbon nanotubes and only Pd catalysts supported on Mo_2C, and they concluded that Mo_2C is not only a support but also a co-catalyst [15]. In addition, Mo_2C is active for hydrogenation and dehydrogenation [16], as well as for low temperature water-gas

* Corresponding author.
E-mail address: haijun.jiao@catalysis.de (H. Jiao).

0378-7753/$ – see front matter © 2013 Elsevier B.V. All rights reserved.
http://dx.doi.org/10.1016/j.jpowsour.2013.07.102

shift (WGS) reaction [17,18]. Transition metal carbides which have the added benefits of lower cost with respect to the Pt group metals, like W_2C and MoC_2have been found to have Pt-like reactivity [19,20].

Theoretically, molybdenum carbides have been used to study various reactions. The hydrogenolysis mechanisms of thiophene [21] and indole [22,23] on clean β-Mo_2C have been studied systematically. The chemisorption and decomposition of small molecules [24–29] such as nitrogenous compounds, aromatic hydrocarbons and CO_2 were examined on both α-Mo_2C and β-Mo_2C phases. Theoretical studies of the chemical properties of methanol [30], methyl iodide [31], CO and the promoting effect of potassium on β-Mo_2C were reported systematically by Pistonesi et al. [32]. Based on their surface experiments; and they found that the incorporation of potassium atoms enhances the dissociation ability of the C–I and C–O bonds in CH_3I and CH_3OH, while blocks the dissociation of CO. Tominaga and Nagai built a schematic potential energy surface for WGS reaction and concluded that CO_2 formation from CO oxidation by surface O is the rate-limiting step [33]. The mechanism of CO hydrogenation and the promoter effect of cobalt have also been systematically reported recently [34]. Liu et al. also calculated WGS mechanism and emphasized the importance of oxygen on the Mo_2C surface [35]. In order to study the intrinsic WGS activities of Mo_2C, Schweitzer et al. loaded Pt on Mo_2C and found Mo_2C to play the role of both support and catalyst [36]. Shi et al. [37] and Han et al. [38] calculated the surface energies of low miller index surfaces of hexagonal Mo_2C to compare their stabilities and concluded that the (011) facet was the most stable surface. The elementary steps of syngas reaction have been systematically studied by using *ab initio* thermodynamics method by Andrew et al. and Mo_2C was proved to have similar catalytic properties with noble metals [39]. Recently, Zheng et al. reported H_2 production from ammonia decomposition catalysed by molybdenum carbide both experimentally and theoretically [40].

In this work, we carried out spin-polarized periodic density functional theory computations to study the adsorption and dissociation of FA on the Mo_2C(101) surface. Our goal is the understanding into the adsorption configurations of FA and its dissociation intermediates on the Mo_2C(101) surface as well as the dissociation paths. These results are compared with those on the Pt group metals, e.g.; Pd(111) [41–44], Pt(111) [43,45,46], and Ir(100) [47], from recent computational studies.

2. Computational details

2.1. Model

Mo_2C mainly has two crystalline structures, the orthorhombic α-Mo_2C phase [48] and the hexagonal β-Mo_2C phase [49,50]. In our work, we used the β-hexagonal Mo_2C phase with an eclipsed configuration as unit cell [51,52]. The calculated lattice parameter of the cell is $2a = 6.075$ Å, $2b = 6.069$ Å and $c = 4.722$ Å, in good agreement with the experiment: $a = b = 3.011$ Å and $c = 4.771$ Å [53]. Among all the surfaces of β-Mo_2C, the (101) surface was reported to be most stable [37,51–55], and there are two types of C atoms and two types of Mo atoms on the exposed surface (Fig. 1). For describing this surface atoms easily, the 4-coordinated (two surface Mo atoms and two bulky phase Mo atoms) C atom is marked as C_A, the 5-coordinated (four surface Mo atoms and one bulky phase Mo atom) C atom is denoted as C_B. The 10-coordinated (three surface Mo atoms, three surface C atoms and four bulky phase Mo atoms) and 11-coordinated (three surface Mo atoms, three surface C atoms and five bulky phase Mo atoms) Mo atoms are notated as Mo_A and Mo_B, respectively. The total supercell contains a $Mo_{32}C_{64}$ unit within a volume of $15.40 \times 12.11 \times 17.96$ Å, and

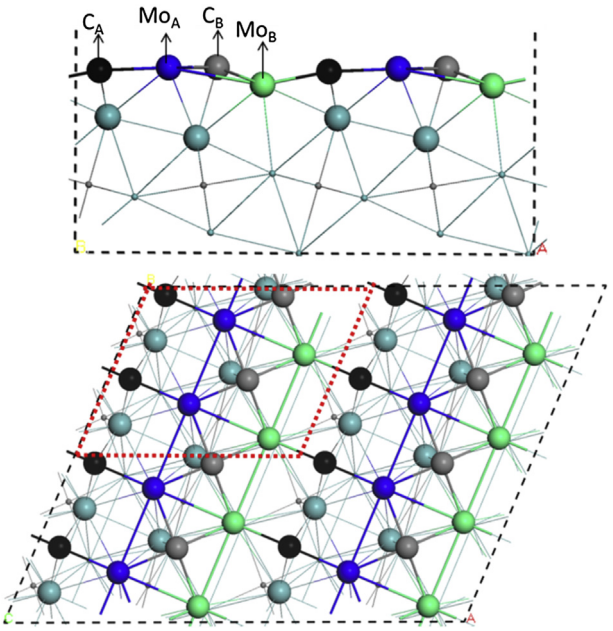

Fig. 1. Side and top views of the Mo_2C(101) surface.

the exposed surface has 16 Mo atoms and 16 C atoms. In addition, a smaller surface model containing 4 exposed Mo atoms and 4 exposed C atoms within the red region of the surface was also employed to study coverage effect, which is defined as the exposed surface Mo atoms, e.g.; 1/16 ML for the large model and 1/4 ML for the small model (Fig. 1).

2.2. Method

All calculations were done using the plane-wave spin-polarized periodic density functional method (DFT) in the Vienna *ab initio* simulation package (VASP) [56–59]. The electron ion interaction was described with the projector augmented wave (PAW) method [60]. The electron exchange and correlation energy was treated within the generalized gradient approximation in the Perdew–Burke–Ernzerhof formalism (GGA-PBE) [61]. For Mo, the core 4p states were also taken into valence region and totally 12 valence electrons were included. The Kohn–Sham one-electron states were expanded in a plane wave with an energy cutoff 400 eV, and the Methfessel–Paxton scheme was used under the electron smearing of $\sigma = 0.1$ eV [62]. The vacuum zone was set up to 12 Å in the z direction to separate the slabs. The geometry optimization was done when force becomes smaller than 0.02 eV $Å^{-1}$ and the energy difference was lower than 10^{-5} eV. For bulk optimization, the lattice parameters were obtained by minimizing the total energy of the unit cell using a conjugated-gradient algorithm to relax the ions and a $5 \times 5 \times 5$ Monkhorst–Pack k-point grid was used for sampling the Brillouin zone [63]. The first Brillouin zone was sampled with $3 \times 3 \times 1$ k-point grid for investigating the surfaces (1/16 and 1/4 ML). The nudged elastic band (NEB) method was used to locate the minimum energy path [64]. The computed vibrational frequencies were used to characterize a minimum state without imaginary frequencies or an authentic transition state with only one imaginary frequency.

The adsorption energy is defined as in Equation, $E_{ads} = E_{A/slab} - [E_{slab} + E_A]$; where $E_{A/slab}$ is the total energy of the slab with adsorbates A, E_{slab} is the total energy of the bare slab, and E_A is the total energy of free adsorbate A in gas phase; and the more negative the E_{ads}, the stronger the adsorption. The activation energy is

defined in Equation, $E_a = E_{TS} - E_{IS}$; and the reaction energy is defined as in Equation, $E_r = E_{FS} - E_{IS}$; where E_{IS}, E_{FS} and E_{TS} represent the total energy of initial, final and transition states.

3. Results and discussion

3.1. Adsorption of the surface intermediates

For each adsorbate, only adsorption site and geometries with the largest adsorption energy are included while many more have been evaluated. Table 1 lists the adsorption energies of the most stable adsorption configurations on the $Mo_2C(101)$ surface at 1/16 ML and 1/4 ML. The rather small differences in adsorption energies of these intermediates show that 1/16 ML is quite larger enough for our analysis and the coverage effects can be ruled out. Fig. 2 shows the most stable adsorption configurations of these intermediates (HCO_2H, CO_2, CO, H_2O, HCO_2, CO_2H, CHO, OH, O and H) at 1/16 ML; and those at 1/4 ML are given in the Supporting information. Our discussion and comparison are mainly based on the data at 1/16 ML, if it is not noted otherwise.

Two FA adsorption configurations on the $Mo_2C(101)$ surface are located, the flat one HCO_2H-flat (**1**) and the perpendicular one HCO_2H–O/OH-down (**2**). As shown in Fig. 2, HCO_2H-flat (**1**) has its O=C–O group chelating with a surface Mo_A atom, and the O atom of the OH group bonding to a neighbouring surface Mo_A atom, and the adsorption energy is −1.12 eV, indicating a strong adsorption. In HCO_2H–O/OH-down (**2**), FA stands over the surface by the O atom of the O=C group interacting with one surface Mo_A atom and the H atom of the OH group pointing towards one surface C_A atom; and the adsorption energy is −1.06 eV, which is only 0.06 eV less stable than that of HCO_2H-flat (**1**). This indicates that both adsorption configurations are very close in energy and they might coexist at this coverage.

CO_2 has two energetically very close adsorption configurations, CO_2–OM/CC (**3**) and CO_2–OM/OM (**4**). In CO_2–OM/CC (**3**), the O atoms bond to surface Mo_A and Mo_B atoms, and the C atom bonds to a surface C_A atom, and the OCO angle is 128.04°; and the adsorption energy is −0.92 eV. In CO_2–OM/OM (**4**), the O atoms bond to surface Mo_A atoms and the C atom bridges two Mo_A atoms, and the OCO angle is 134.96°; and the adsorption energy is −0.81 eV. In addition, the physisorption is also located and the adsorption energy is only −0.19 eV, much weaker than the chemisorption.

CO has two energetically almost equivalent configurations, CO-flat (**5**) and CO–C-down (**6**). In CO-flat (**5**), the O atom bonds to two surface Mo_A atoms, and the C atom bonds to two surface C_A atoms; and the adsorption energy is −1.61 eV. In CO–C-down (**6**), the C atom adsorbs vertically atop on one surface Mo_A atom, and the adsorption energy is −1.58 eV.

H_2O (**7**) prefers the O atom bonding to surface Mo_A atom, and its H atoms pointing towards a neighbouring C_A and a neighbouring Mo_A atom, and the adsorption energy is −0.66 eV.

The most stable adsorption configurations of formate are HCO_2–O/O-down (**8**), HCO_2-flat (**9**) and HCO_2–O/H-down (**10**). In HCO_2–O/O-down (**8**), HCO_2 stands perpendicular to the surface and the O atoms bridge two surface Mo_A atoms with O–Mo_A distances of 215 pm; and the adsorption energy is −4.04 eV. In HCO_2-flat (**9**), HCO_2 covers the surface and its two O atoms bond directly to two Mo_A atoms with the Mo–O distances of 203 pm; and the adsorption energy is −3.44 eV. In HCO_2–O/H-down (**10**), one of its O atoms bonds to a surface Mo_A atom with the O–Mo_A distance of 207 pm and the H atom points towards the neighbouring Mo_A with the H–Mo_A distance of 222 pm; and the adsorption energy is −2.88 eV. These show that HCO_2–O/O-down (**8**) is the most stable adsorption configuration.

Carboxyl (CO_2H) has two energetically very close adsorption configurations, CO_2H–OM/CC (**11**) and CO_2H–OM/CM (**12**). In CO_2H–OM/CC (**11**), the O atom of the O=C group interacts with one surface Mo_A atom and the C atom binds to one neighbouring surface C_A atom as well as the H atom points to one surface C_A atom (the configuration with the H atom opposite to the surface C_A atom is 0.03 eV less stable, Supporting information); and the adsorption energy is −2.92 eV. In CO_2H–OM/CM (**12**), the O=C group bridges two surface Mo_A atoms and the H atom is opposite to the surface (the configuration with the H atom pointing to the surface is 0.04 eV less stable, Supporting information) and the adsorption energy is −2.85 eV. These indicate their possible co-existence.

Formyl (CHO, **13**) prefers the O atom bridging two neighbouring surface Mo_A atoms and the C atom bridging one Mo_A and one surface C_A; and the adsorption energy is −3.22 eV. Hydroxyl (OH, **14**) has its O atom bridging two neighbouring surface Mo_A atoms, and the adsorption energy is −4.15 eV. Atomic oxygen (O, **15**) has atop adsorption on one surface Mo_A atom, and the adsorption energy is −6.59 eV; and atomic hydrogen (H, **16**) has atop adsorption on one surface C_A atom and the adsorption energy is −2.79 eV.

Table 1
The computed adsorption energies (E_{ads}, eV) for the most stable adsorption configurations of the intermediates involved in FA dissociation at 1/16 and 1/4 ML.

Species	1/16 ML	1/4 ML
HCO_2H-flat (**1**)	−1.12	−1.16
HCO_2H–O/OH-down (**2**)	−1.06	−1.06
CO_2–OM/CC (**3**)	−0.92	−0.87
CO_2–OM/OM (**4**)	−0.81	−0.81
CO-flat (**5**)	−1.61	−1.32
CO–C-down (**6**)	−1.58	−1.56
H_2O (**7**)	−0.66	−0.63
HCO_2–O/O-down (**8**)	−4.04	−4.10
HCO_2-flat (**9**)	−3.44	−3.54
HCO_2–O/H-down (**10**)	−2.88	−2.76
CO_2H–OM/CC (**11**)	−2.92	−2.91
CO_2H–OM/CM (**12**)	−2.85	−2.94
CHO (**13**)	−3.22	−3.21
OH (**14**)	−4.15	−4.16
O (**15**)	−6.59	−6.58
H (**16**)	−2.79	−2.76

3.2. Dissociation path

On the basis of the above discussed adsorption configurations and energies, we analyzed FA dissociation on the surface starting from the two most stable HCO_2H-flat (**1**) and HCO_2H–O/OH-down (**2**). The adsorption configuration of the transition states are shown in Fig. 3; and the energetic parameters are given in Table 2.

(a) FA dissociation: Since FA has two adsorption configurations in close energy; we studied both dissociation routes accordingly. Starting from HCO_2H-flat (**1**), FA can dissociate either to HCO_2 + H (formate) or alternatively to CO_2H + H (carboxyl) or to CHO + OH (formyl + hydroxyl). For HCO_2 formation, the transition state TS(HCO_2H-flat/HCO_2 + H) (**a**) is located, and the breaking O–H distance is 137 pm and the forming C_B–H distance is also 137 pm. The energy barrier is 0.93 eV and the reaction is exothermic by 1.12 eV. For CO_2H formation, the transition state TS(HCO_2H-flat/H + CO_2H) (**b**) is located; and the breaking C–H distance is 149 pm and the forming C_A–H distance is 137 pm. The energy barrier is 1.47 eV, which is 0.35 eV higher than the adsorption of FA (−1.12 eV); and the reaction is exothermic by 0.23 eV. For FA dissociation into CHO + OH, the transition state TS(HCO_2H-flat/CHO + OH) (**c**) is located; and the breaking C–O distance is 210 pm (146 pm in HCO_2H-flat (**1**)). The energy barrier is 0.48 eV and the reaction is exothermic by 1.16. It is clearly to see that starting from

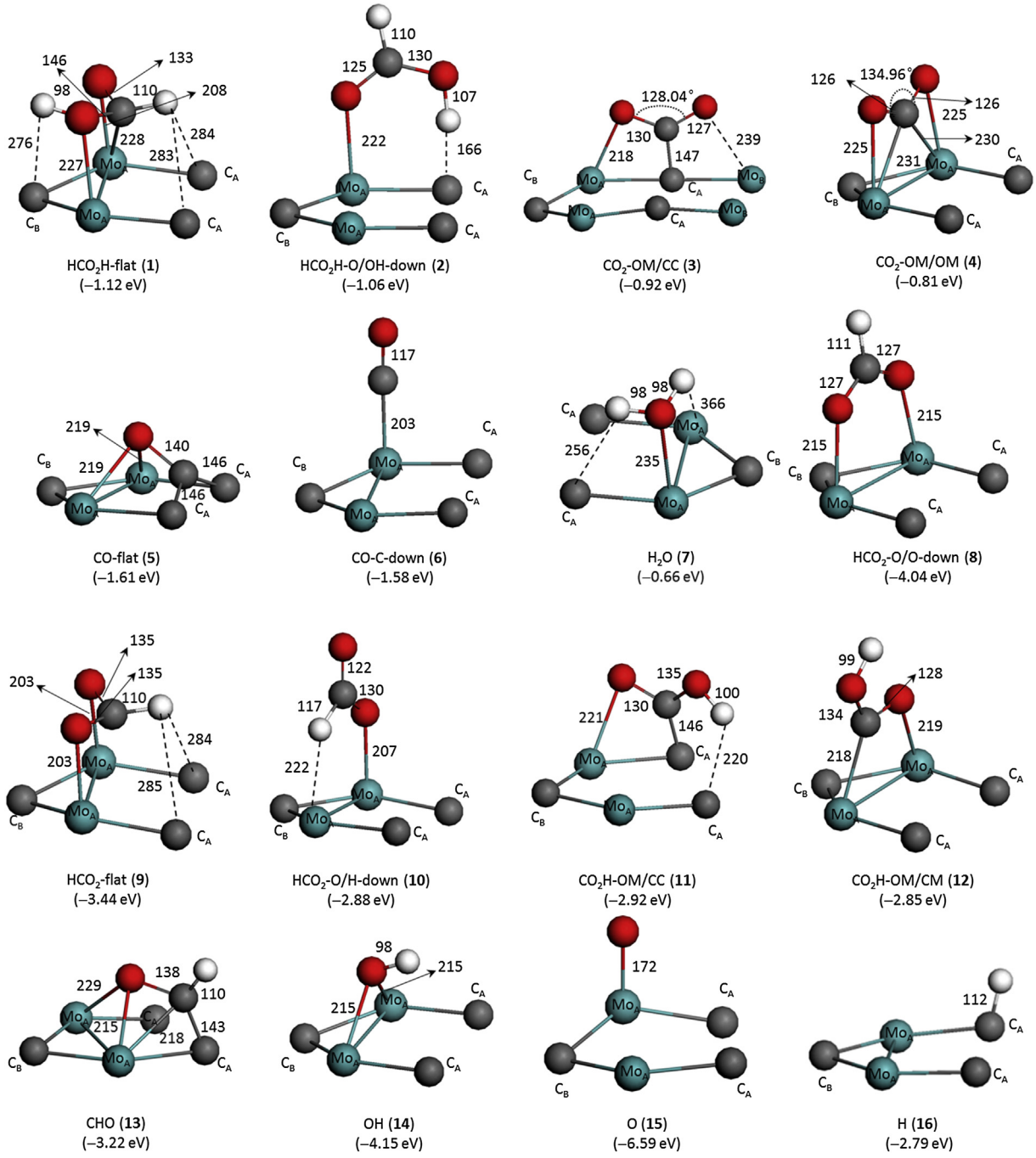

Fig. 2. The most stable adsorption configurations of intermediates involved in FA decomposition.

HCO_2H-flat (**1**) FA prefers to dissociate into CHO + OH rather than into HCO_2 + H or CO_2H + H both thermodynamically and kinetically. Starting from HCO_2H–O/OH-down (**2**), FA can only dissociate into HCO_2 + H because of its perpendicular adsorption configuration. In the transition state TS(HCO_2H–O/OH-down/H + HCO_2) (**d**), the breaking O–H distance is elongated to 122 pm and the forming H–C_A bond is 140 pm (107 and 166 pm in HCO_2H–O/OH-down (**2**), respectively); and the energy barrier is only 0.02 eV and the reaction energy is exothermic by 1.18 eV. This shows that FA dissociates spontaneously into HCO_2 + H. Compared to the adsorption energy and the dissociation barriers of HCO_2H-flat (**1**), HCO_2H–O/OH-down (**2**) dissociation into HCO_2 + H is much more favourable kinetically.

To show this preference more clearly, we calculated the FA adsorption at very high coverage (1/2 ML); and only HCO_2H–O/OH-down (**2**) adsorption configuration is possible, and the computed FA adsorption energy is −0.80 eV, which is lower than that of the first FA adsorption at 1/4 ML, indicating a significant lateral repulsive interaction of 0.26 eV. At such high coverage, HCO_2H–O/OH-down (**2**) dissociation into HCO_2 + H is the only possible route.

(b) HCO_2 dissociation: As the most favourable surface intermediate, formate dissociation into either O + CHO or H + CO_2 was studied. For the O + CHO route from HCO_2–O/O-down (**8**), the transition state TS(HCO_2–O/O-down/O + CHO) (**e**) is located; the breaking C–O bond distance is elongated from 127 pm to 143 pm and the energy barrier is 2.27 eV and the reaction is thermal neutral

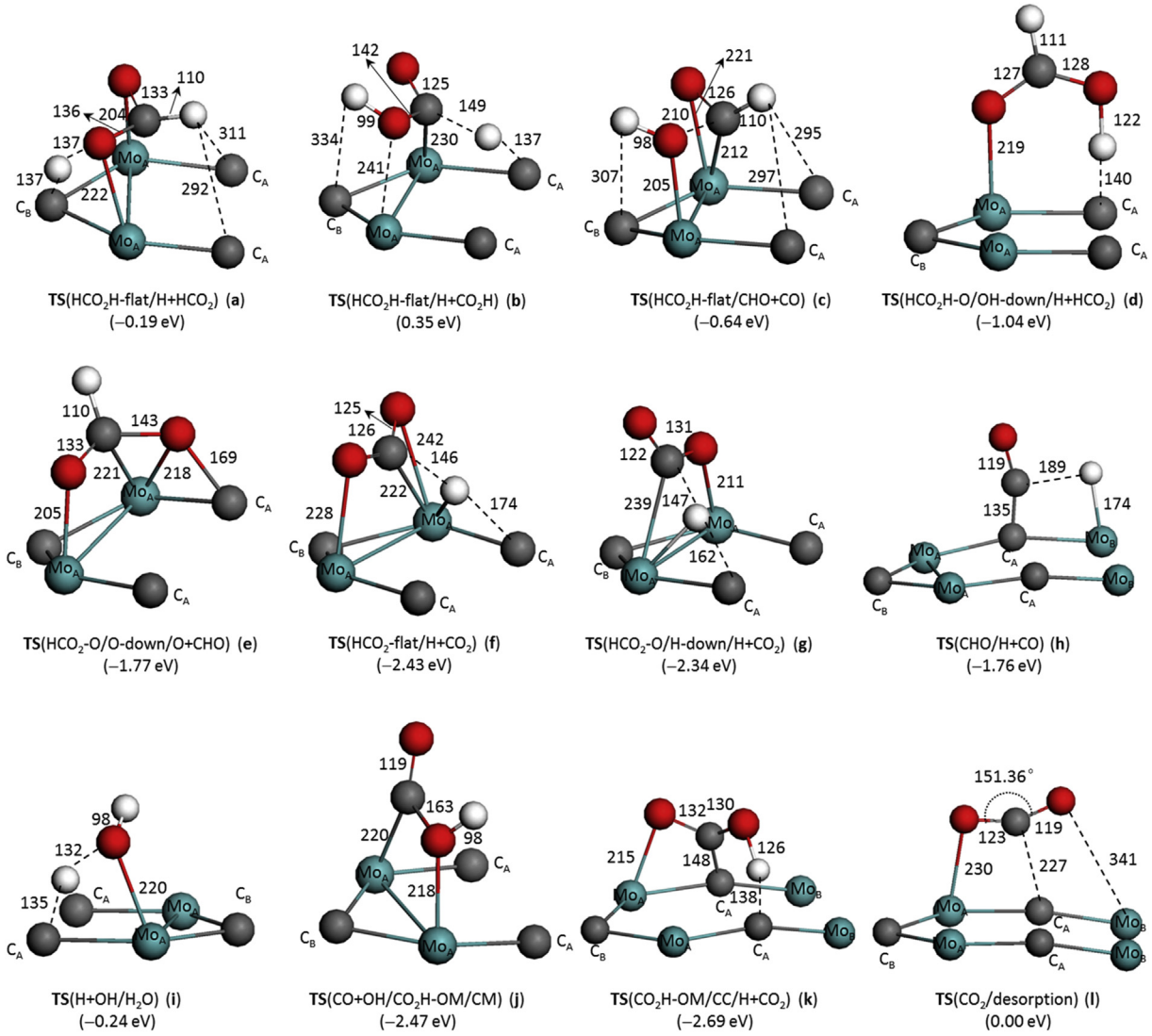

Fig. 3. The transition state configurations involved in FA decomposition.

(−0.02 eV). For the CO_2 + H route from HCO_2–O/O-down (**8**), it is not possible for a direct C–H bond dissociation due to its perpendicular orientation, and the less stable adsorption configurations, HCO_2-flat (**9**) and HCO_2–O/H-down (**10**) from the dynamic bending were considered [65–69]. Starting from HCO_2-flat (**9**) into CO_2 + H, the transition state TS(HCO_2-flat/H + CO_2) (**f**) is located; where the breaking C–H distance is 146 pm and the forming C_A–H distance is 174 pm. The energy barrier is 1.01 eV. Starting from HCO_2–O/H-down (**10**) into CO_2 + H, the transition state TS(HCO_2–O/H-down/H + CO_2) (**g**) is located; where the breaking C–H distance is 147 pm and the forming C_A–H distance is 162 pm. The energy barrier is 0.54 eV.

Table 2
The computed energy barriers (E_a, eV) and reaction energies (E_r, eV) for the elementary steps of FA dissociation.

Reaction	E_a/E_r	
	1/16 ML	1/4 ML
HCO_2H-flat/H + HCO_2 (**a**)	0.93/−1.12	0.95/−1.11
HCO_2H-flat/H + CO_2H (**b**)	1.47/−0.23	1.49/−0.16
HCO_2H-flat/CHO + CO (**c**)	0.48/−1.16	0.49/−1.12
HCO_2H–O/OH-down/H + HCO_2 (**d**)	0.02/−1.18	0.01/−1.21
HCO_2–O/O-down/O + CHO (**e**)	2.27/−0.02	2.27/−0.04
HCO_2-flat/H + CO_2 (**f**)	1.01/−0.26	1.17/−0.07
HCO_2–O/H-down/H + CO_2 (**g**)	0.54/−0.82	0.54/−0.85
CHO/H + CO (**h**)	1.46/−0.02	1.53/0.05
H + OH/H_2O (**i**)	1.36/0.94	1.31/0.95
CO + OH/CO_2H–OM/CM (**j**)	1.40/1.02	1.27/0.89
CO_2H–OM/CC/H + CO_2 (**k**)	0.23/−0.55	0.27/−0.47
CO_2/desorption (**l**)	0.92	0.87

Starting from HCO_2–O/O-down (**8**), the effective barrier via the transition state TS(HCO_2-flat/H + CO_2) (**f**) is 1.61 eV; while the effective barrier via the transition state TS(HCO_2–O/H-down/H + CO_2) (**g**) is 1.70 eV; and the reaction is endothermic by 0.34 eV. Compared with the high barrier (2.27 eV) of O + CHO formation, the formation of H + CO_2 via the dynamic bending HCO_2-flat (**9**) configuration is more favourable kinetically.

(c) CHO dissociation as well as H_2O and CO_2 formation: As the most favourable route for CHO + OH formation from HCO_2H-flat (**1**), we computed CHO (**13**) dissociation into CO + H, and the subsequent CO_2H formation from CO + OH as well as H_2O formation from H + OH. For CHO dissociation into CO + H, the transition state TS(CHO/H + CO) (**h**) is located, and the C–H distance is 189 pm; and the energy barrier is 1.46 eV and the reaction is almost thermal neutral (−0.02 eV).

Starting from the previously formed surface OH, the further reactions of CO + H into H_2O and CO_2H were calculated. For H_2O (**7**) formation from H + OH, the transition state TS(H + OH/H_2O) (**i**) is located, and the forming O–H distance is 132 pm and the breaking surface C–H distance is 135 pm; and the energy barrier is 1.36 eV and the reaction is endothermic by 0.94 eV, while the back reaction has lower energy barrier of 0.42 eV. Therefore, H_2O dissociation is more favourable than its formation.

For CO_2H formation from CO + OH, the transition state TS(CO + OH/CO_2H–OM/CM) (**j**) is located, and the forming C–O distance is 163 pm, and the energy barrier is 1.40 eV; and the reaction is endothermic by 1.02 eV; while the back reaction has lower energy barrier of 0.38 eV; these show that CO_2H dissociation instead of formation is more favourable. Nevertheless, we also calculated CO_2H dissociation into CO_2 + H. It is to note that there are two adsorption configurations for CO_2H in very close energy, CO_2H–OM/CC (**11**) and CO_2H–OM/CM (**12**). Starting from the more stable CO_2H–OM/CC (**11**), we located the transition state TS(CO_2H–OM/CC/H + CO_2) (**k**), in which the breaking H–O distance is 126 pm and the forming H–C_A distance is 138 pm; and the energy barrier is 0.23 eV; and the reaction is exothermic by 0.55 eV. In addition, CO_2H–OM/CM (**12**) (Supporting information) dissociates into CO_2 + H is less favourable kinetically.

On the basis of the computed energy barriers and the reaction energies for CO_2H formation and dissociation, CO_2H dissociation into CO_2 + H is kinetically more favourable, while CO_2H dissociation back to CO + OH is kinetically less favourable, but thermodynamically more favourable.

(d) CO_2 desorption: Since CO_2 has a strong adsorption on the surface, the corresponding desorption was computed. Starting from the most stable adsorption configuration (CO_2–OM/CC (**3**)), the transition state TS(CO_2/desorption) (**l**) is located; in which the distance of O–Mo_A and C–C_A is 230 and 227 pm, respectively; and the OCO angle is 151.36°, which is larger than that (128.04°) in CO_2–OM/CC (**3**); and the desorption energy is endothermic by 0.92 eV, and this is also the CO_2 adsorption energy.

The computed adsorption energies of the intermediates involved in FA dissociation in Table 1 show negligible differences between 1/16 ML and 1/4 ML apart from the flat adsorbed CO (**5**), which has a difference of 0.29 eV. Detailed analysis into this difference shows the strong reconstruction of the surface structure for CO (**5**) at 1/4 ML and no such significant surface reconstructions can be found for other intermediates. Similar coverage effects have also been found for the energy barriers and reaction energies for the elemental steps for FA dissociation (Table 2). All these show that our surface models are large enough for computing FA dissociation.

3.3. Potential energy surface

On the basis of the computed energetic parameters for the elementary steps, we have mapped the potential energy surface for FA adsorption and decomposition on the Mo_2C(101) at 1/16 ML (Fig. 4). FA has two adsorption configurations close in energy, parallel to the surface (HCO_2H-flat (1, $E_{ads} = -1.12$ eV)) and perpendicular to the surface (HCO_2H–O/OH-down (2, $E_{ads} = -1.06$ eV)). However, they have very different dissociation routes. Starting from the more stable configuration (**1**), a potential route follows its dissociation (**c**) forming surface CHO and OH (CHO + OH). Other dissociation routes towards surface formate (HCO_2) (**a**) and carboxyl (CO_2H) (**b**) have much higher barriers and thus kinetically much less favoured. Considering (**2**), which is a less stable configuration than (**1**), the formation of surface formate (**8**) proceeds almost barrier-less following the dissociation route (**d**). We shall revisit this result when discussing the selectivity.

Continuing the reaction pathway starting at (**8**), direct C–H bond cleavage is not possible. Also the dissociation of (**8**) into surface CHO + O is not competitive, as its barrier is 2.27 eV. Instead, dynamic bending involving the adsorption configurations HCO_2-falt (**9**) and HCO_2–O/H-down (**10**) become likely. These processes need to overcome an effective barrier of 1.70 eV, and the surface CO_2 formation is endothermic by 0.34 eV (or 1.26 eV to gaseous CO_2). However, the overall reaction pathway remains below the potential energy of the initial state (FA in gas phase ($E \equiv 0.00$ eV)).

A potential competitive reaction pathway may start at the surface CHO (**13**). The dissociation of (**13**) into surface CO + H is associated with a barrier of 1.46 eV, and the reaction is nearly thermal neutral. The subsequent elementary steps of CO and OH to form surface carboxyl (**12**) as well as H + OH to form surface H_2O

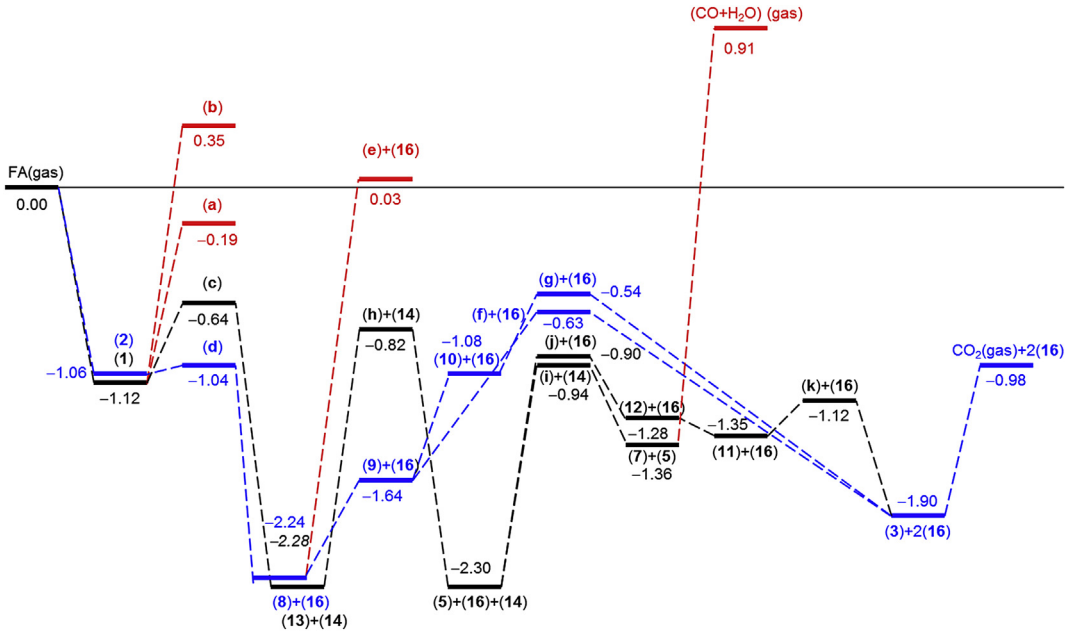

Fig. 4. The potential energy surface for FA dissociation at 1/16 ML on the Mo_2C(101) surface starting from gaseous FA.

Table 3
Comparison of the adsorption energies (E_{ads}, eV), dissociation barriers (E_a, eV) and dissociation energies (E_r, eV) of FA on β-M_2C(101), Pd(111) and Pt(111) as well as on Ir(100) surfaces.

	Mo_2C(101)	Pd(111)	Pt(111)	Ir(100)
E_{ads} (HCO_2H)	−1.12; −1.06	−0.39 [41]; −0.62 [42]; −0.40 [43]; −0.40 [44]	−0.39 [43]; −0.40/−0.34 [45]; −0.26 [46]	−0.63 [47]
E_{ads} (HCO_2)	−4.04	−2.37 [41]; −2.71 [42]; −2.52 [43]; −2.49 [44]	−2.27 [43]; −2.32/−2.50 [45]	−3.66 [47]
E_{ads} (CO_2)[a]	−0.92	0.23 [41]		
E_{ads} (H)	−2.79	−2.78 [41]; −2.92 [42]; −2.89 [43]	−2.78 [43]	−3.01 [47]
E_a ($HCO_2H \rightarrow HCO_2 + H$)	0.02	0.58 [41]; 1.00 [42]; 0.68 [43]; 0.49 [44]	0.72 [46]; 0.94/0.88 [45]; 0.69 [43]	
E_r ($HCO_2H \rightarrow HCO_2 + H$)	−1.18	−0.17 [41]; 0.00 [42]; −0.27 [43]; −0.09 [44]	0.03 [43]	0.18 [47]
E_a ($HCO_2 \rightarrow CO_2 + H$)[b]	1.61	0.76 [41]; 0.88 [42]; 1.59 [43]; 0.77 [44]	1.23 [46]; 1.56/1.16 [45]; 1.88 [43]	0.87 [47]
E_r ($HCO_2 \rightarrow CO_2 + H$)	0.34	−0.43 [41]; −0.29 [42]; −0.45 [43]; −0.22 [44]	−0.43 [43]; −0.31/−0.63 [45]	−0.06 [47]
Supercell	(4 × 4)	(3 × 3) [41]; (3 × 3) [42]; (3 × 3) [43]; (3 × 3) [44]	(2 × 4) [46]; (3 × 3/2 × 2) [45]; (3 × 3) [43]	(3 × 3) [47]

[a] Chemisorption state energy.
[b] Effective energy barrier.

(**7**) need high barriers (1.40 eV and 1.36 eV, respectively) and are endothermic by 1.02 and 0.94 eV, respectively. These show that (**12**) and (**7**) are metal-stable intermediates and they prefer the dissociation into surface CO (**5**) and OH. However, desorption of CO and H_2O is highly endothermic and would thus lead to poisoning of the active sites. Since the elementary steps are equilibrated, this part of the reaction may also proceed in the reverse direction.

With a view to the high selectivity the catalyst provides for the overall decomposition of FA towards CO_2 and H_2, we should keep in mind that the entire potential energy surface remains below the potential energy of FA; all elementary steps are equilibrated. Additionally, we may formulate the conservation of the number of active sites by the sum of all intermediates sticking to the surface, which is constant. Due to the thermodynamic equilibrium, the equation is cancelling down to $1 = \theta_{HCO_2+H} + \theta_{CHO+OH}$, where θ is the coverage. Although the reaction pathway via (**13**) also lead to CO_2 formation, the probability is very low. Reason for this observation is the barrier of the elementary step (**c**), which is higher and requires a $\sim 10^6$ times longer lifetime of the transition state than that of (**d**). Finally, the overall reaction rate for FA decomposition via the HCO_2 pathway was found to be 2300 times faster than that following the HCO pathway (Supporting information).

Fig. 4 illustrates the potential energy surface and highlights the most favourable route of the decomposition of FA via formate towards CO_2 + 2H (blue line in web version). This agrees with the experimental findings of CO-free H_2 [14].

3.4. Comparison with Pd(111), Pt(111) and Ir(100)

Since molybdenum carbide has been proposed to have the catalytic activity of the Pt group metals, we compared the energetic parameters of FA adsorption and dissociation on Mo_2C(101), Pt(111), Pd(111) and Ir(100). Since the formate route is the more preferable mechanism, it is much easy for the general comparison, and these data are summarized in Table 3.

As shown in Table 3, FA has much stronger adsorption energy on Mo_2C(101) than on Pd(111), Pt(111) and Ir(100); all these surfaces have FA chemisorption. For CO_2 adsorption, there are quite large differences among these surfaces. For example, CO_2 on Mo_2C(101) has much stronger chemisorption energy, while Pd(111) does not adsorb CO_2 (positive adsorption energies).

For hydrogen atom adsorption, all these surfaces have very close adsorption energies in the range of −2.8 to −3.0 eV; and there are no differences among these surfaces apart from the fact that H adsorption prefers the surface carbon atom instead of surface Mo atom. For formate adsorption, Mo_2C(101) has stronger chemisorption energy than Pd(111), Pt(111) and Ir(100).

For FA dissociation into surface formate and hydrogen, Pd(111) and Pt(111) have very high activation barriers, while Mo_2C(101) is practically barrier-less. Along with the energy barriers, FA dissociation into surface formate and hydrogen is strongly exothermic on Mo_2C(101), and almost thermal neutral on Pd(111) and Pt(111). It is endothermic on Ir(100). For formate dissociation into surface CO_2 and hydrogen, Mo_2C(101) has very high effective barrier, while Pd(111), Pt(111) and Ir(100) have low effective barrier apart from the reported 1.59 and 1.88 eV for Pd(111) and Pt(111) by Hu et al. [43], respectively. The corresponding dissociation energy is endothermic on Mo_2C(101), while strongly exothermic on Pd(111) and Pt(111).

4. Conclusions

For the catalytic and selective decomposition of formic acid into CO_2 and hydrogen on β-Mo_2C(101), the adsorption configurations and energies of the surface intermediates (HCO_2H, CO_2, CO, H_2O, HCO_2, CO_2H, CHO, OH, O and H) have been computed systematically. On the basis of the most stable adsorption states the full potential energy surface has been mapped and the minimum energy path has been identified.

Among the three possibilities for the first step dissociation of formic acid dissociation (CHO + OH, HCO_2 + H and CO_2H + H), the formate route is most favourable, and surface formate from HCO_2H–O/OH-down (**2**) represents the most important intermediate and the most stable adsorption configuration HCO_2–O/O-down (**8**) has its two oxygen atoms bridging two surface Mo_A atoms.

Starting from HCO_2–O/O-down (**8**), formate dissociation into CO_2 and hydrogen is kinetically much more favoured than into surface formyl and oxygen (CHO + O). Formate dissociation into CO_2 and hydrogen is the rate-determining step and HCO_2–O/O-down (**8**) represents the resting state. Our results rule out the possible formation of CO and H_2O, and Mo_2C exhibits a unique property to catalyse formic acid dissociation into CO-free hydrogen.

Because of the proposed Pt-like properties for transition metal carbides, the adsorption properties of HCO_2H, HCO_2, CO_2 and H as well as their dissociation energetic on Mo_2C(101) have been compared with those on Pd(111), Pt(111) and Ir(100). Apart from the adsorption of hydrogen atom, which has very close adsorption energies on all these surfaces, Mo_2C(101) can adsorb these intermediates much stronger than Pd(111) and Pt(111), in particularly the much stronger CO_2 chemisorption.

For the first step of formic acid dissociation into surface formate and hydrogen on Mo_2C(101), it is barrier-less and highly exothermic, while it has higher barriers and is less exothermic on Pd(111) and Pt(111). Due to the much stronger adsorption of surface formate, the dissociation of formate into surface CO_2 and hydrogen has higher effective barrier, while this dissociation step on Pd and Pt has lower barrier.

Acknowledgement

This work was supported by the China Scholarship Council (to Q. Luo). We also acknowledge general finical support from the BMBF and the State of Mecklenburg-Western Pommerania.

Appendix A. Supplementary data

It is to note that a review article about formic acid adsorption and decomposition on a set of metals and metal oxides has been published very recently. (http://dx.doi.org/10.1142/S0219633613300012).

Supplementary data related to this article can be found at http://dx.doi.org/10.1016/j.jpowsour.2013.07.102.

References

[1] B. Loges, A. Boddien, F. Gärtner, H. Junge, M. Beller, Top. Catal. 53 (2010) 902–914.
[2] M. Grasemann, G. Laurenczy, Energy Environ. Sci. 5 (2012) 8171–8181.
[3] F. Joó, ChemSusChem 1 (2008) 805–808.
[4] K. Tedsree, C.W.A. Chan, S. Jones, Q. Cuan, W.-K. Li, X.-Q. Gong, S.C.E. Tsang, Science 332 (2011) 224–228.
[5] K. Tedsree, T. Li, S. Jones, C.W.A. Chan, K.M.K. Yu, P.A.J. Bagot, E.A. Marquis, G.D.W. Smith, S.C.E. Tsang, Nat. Nanotechnol. 6 (2011) 302–306.
[6] Q.-Y. Bi, X.-L. Du, Y.-M. Liu, Y. Cao, H.-Y. He, K.-N. Fan, J. Am. Chem. Soc. 134 (2012) 8926–8933.
[7] X. Gu, Z.-H. Lu, H.-L. Jiang, T. Akita, Q. Xu, J. Am. Chem. Soc. 133 (2011) 11822–11825.
[8] B. Loges, A. Boddien, F. Gärtner, H. Junge, M. Beller, Angew. Chem. Int. Ed. 47 (2008) 3962–3965.
[9] C. Fellay, P.J. Dyson, G. Laurenczy, Angew. Chem. Int. Ed. 47 (2008) 3966–3968.
[10] S. Fukuzumi, Eur. J. Inorg. Chem. (2008) 1351–1362.
[11] T.R. Johnson, D.J. Morris, M. Wills, Chem. Soc. Rev. 39 (2010) 81–88.
[12] A. Boddien, D. Mellmann, F. Gärtner, R. Jackstell, H. Junge, P.J. Dyson, G. Laurenczy, R. Ludwig, M. Beller, Science 333 (2011) 1733–1736.
[13] D.W. Flaherty, S.P. Berglund, C.B. Mullins, J. Catal. 269 (2010) 33–43.
[14] À. Koós, F. Solymosi, Catal. Lett. 138 (2010) 23–27.
[15] Z. Cui, C. Gong, C.X. Guo, C.M. Li, J. Mater. Chem. A 1 (2013) 1179–1184.
[16] H.H. Hwu, J.G. Chen, Chem. Rev. 105 (2005) 185–212.
[17] J.A. Schaidle, A.C. Lausche, L.T. Thompson, J. Catal. 272 (2010) 235–245.
[18] M. Nagai, K. Matsuda, J. Catal. 238 (2006) 489–496.
[19] R.L. Levy, M. Boudart, Science 181 (1973) 547–549.
[20] J.G. Chen, Chem. Rev. 96 (1996) 1447–1498.
[21] H. Tominaga, M. Nagai, Appl. Catal. A 343 (2008) 95–103.
[22] W. Piskorz, G. Adamski, A. Kotarba, Z. Sojka, C. Sayag, G. Djega-Mariadassou, Catal. Today 119 (2007) 39–43.
[23] A. Kotarba, G. Adamski, W. Piskorz, Z. Sojka, C. Sayag, G. Djega-Mariadassou, J. Phys. Chem. B 108 (2004) 2885–2892.
[24] M. Nagai, H. Tominaga, S. Omi, Langmuir 16 (2000) 10215–10220.
[25] J. Ren, C.F. Huo, J.G. Wang, Y.W. Li, H. Jiao, Surf. Sci. 596 (2005) 212–221.
[26] J. Ren, C.F. Huo, J.G. Wang, Z. Cao, Y.W. Li, H. Jiao, Surf. Sci. 600 (2006) 2329–2337.
[27] J. Ren, J.G. Wang, C.F. Huo, X.D. Wen, Z. Cao, S.P. Yuan, Y.W. Li, H. Jiao, Surf. Sci. 601 (2007) 1599–1607.
[28] A.S. Rocha, A.B. Rocha, V.T. Silva, Appl. Catal. A 379 (2010) 54–60.
[29] X.R. Shi, J.G. Wang, K. Hermann, J. Phys. Chem. C 114 (2010) 13630–13641.
[30] C. Pistonesi, A. Juan, A.P. Farkas, F. Solymosi, Surf. Sci. 602 (2008) 2206–2211.
[31] M.E. Pronsato, C. Pistonesi, A. Juan, A.P. Farkas, L. Bugyi, F. Solymosi, J. Phys. Chem. C 115 (2011) 2798–2804.
[32] C. Pistonesi, M.E. Pronsato, L. Bugyi, A. Juan, J. Phys. Chem. C 116 (2012) 24573–24581.
[33] H. Tominaga, M. Nagai, J. Phys. Chem. B 109 (2005) 20415–20423.
[34] H. Tominaga, Y. Aoki, M. Nagai, Appl. Catal. A 423 (2012) 192–204.
[35] P. Liu, J.A. Rodriguez, J. Phys. Chem. B 110 (2006) 19418–19425.
[36] N.M. Schweitzer, J.A. Schaidle, O.K. Ezekoye, X.Q. Pan, S. Linic, L.T. Thompson, J. Am. Chem. Soc. 133 (2011) 2378–2381.
[37] X.R. Shi, S.G. Wang, H. Wang, C.M. Deng, Z.F. Qin, J.G. Wang, Surf. Sci. 603 (2009) 852–859.
[38] J.W. Han, L. Li, D.S. Sholl, J. Phys. Chem. C 115 (2011) 6870–6876.
[39] A.J. Medford, A. Vojvodic, F. Studt, F. Abild-Pedersen, J.K. Nørskov, J. Catal. 290 (2012) 108–117.
[40] W. Zheng, T.P. Cotter, P. Kaghazchi, T. Jacob, B. Frank, K. Schlichte, W. Zhang, D.S. Su, F. Schuth, R. Schlogl, J. Am. Chem. Soc. 135 (2013) 3458–3464.
[41] Q. Luo, G. Feng, M. Beller, H. Jiao, J. Phys. Chem. C 116 (2012) 4149–4156.
[42] R. Zhang, H. Liu, B. Wang, L. Ling, J. Phys. Chem. C 116 (2012) 22266–22280.
[43] C. Hu, S.-W. Ting, K.-Y. Chan, W. Huang, Int. J. Hydrogen Energy 37 (2012) 15956–15965.
[44] D.W. Yuan, Z.R. Liu, J. Power Sources 224 (2013) 241–249.
[45] W. Gao, J.A. Keith, J. Anton, T. Jacob, Dalton Trans. 39 (2010) 8450–8456.
[46] Y. Kang, L. Qi, M. Li, R.E. Diaz, D. Su, R.R. Adzic, E. Stach, J. Li, C.B. Murray, ACS Nano 6 (2012) 2818–2825.
[47] X. Li, K.H. Lim, ChemCatChem 4 (2012) 1311–1320.
[48] C. Pistonesi, A. Juan, A.P. Farkas, F. Solymosi, Surf. Sci. 604 (2010) 914–919.
[49] J. Dubois, T. Epicier, C. Esnouf, G. Fantozzi, P. Convert, Acta Metall. 8 (1988) 1891–1901.
[50] T. Epicier, J. Dubois, C. Esnouf, G. Fantozzi, P. Convert, Acta Metall. 8 (1988) 1903–1921.
[51] T. Wang, X.W. Liu, S.G. Wang, C.F. Huo, Y.-W. Li, J. Wang, H. Jiao, J. Phys. Chem. C 115 (2011) 22360–22368.
[52] J. Haines, J.M. Leger, C. Château, J.E. Lowther, J. Phys. Condens. Mater. 13 (2001) 2447–2454.
[53] E. Rudy, S. Windisch, A.J. Stosick, J.R. Hoffman, Trans. Metall. Soc. AIME 239 (1967) 1247–1267.
[54] X.H. Wang, H.L. Hao, M.H. Zhang, W. Li, K.Y. Tao, J. Solid State Chem. 179 (2006) 538–543.
[55] M. Nagai, A.M. Zahidul, K. Matsuda, Appl. Catal. A 313 (2006) 137–145.
[56] G. Kresse, J. Hafner, Phys. Rev. B 47 (1993) 558–561.
[57] G. Kresse, J. Hafner, Phys. Rev. B 49 (1994) 14251–14269.
[58] G. Kresse, J. Furthmüller, Comput. Mater. Sci. 6 (1996) 15–50.
[59] G. Kresse, J. Furthmüller, Phys. Rev. B 54 (1996) 11169–11186.
[60] P.E. Blöchl, Phys. Rev. B 50 (1994) 17953–17979.
[61] J.P. Perdew, K. Bruke, M. Ernzerhof, Phys. Rev. Lett. 77 (1996) 3865–3868.
[62] M. Methfessel, A.T. Paxton, Phys. Rev. B 40 (1989) 3616–3621.
[63] M. Monkhorst, J.D. Pack, Phys. Rev. B 13 (1976) 5188–5192.
[64] H. Jónsson, G. Mills, K.W. Jacobsen, in: B.J. Berne, D.F. Ciccotti (Eds.), Classical and Quantum Dynamics in Condensed Phase Simulations, World Scientific, Singapore, 1998, p. 385.
[65] H. Nakatsuji, M. Yoshimoto, M. Hada, K. Domen, C. Hirose, Surf. Sci. 336 (1995) 232–244.
[66] H. Nakatsuji, M. Yoshimoto, Y. Umemura, S. Takagi, M. Hada, J. Phys. Chem. 100 (1996) 694–700.
[67] M. Yoshimoto, S. Takagi, Y. Umemura, M. Hada, H. Nakatsuji, J. Catal. 173 (1998) 53–63.
[68] M. Lintuluoto, H. Nakatsuji, M. Hada, H. Kanai, Surf. Sci. 429 (1999) 133–142.
[69] P. Persson, S. Lunell, L. Ojamaee, Int. J. Quantum Chem. 89 (2002) 172–180.